12 Technology of SS-OCT Biometer: Argos Biometer

Changho Chong

Background

Optical coherence tomography was developed by two groups, D. Hwang and J. Fujimoto in MIT in 1990 [1], Japanese researcher, Tanno in 1989, almost simultaneously but independently. Since it was commercialized for retinal imaging in 1994, it has been indispensable diagnostic modality for early diagnosis of retinal diseases in ophthalmic practice. Some years later, Swept Source-Optical Coherence Tomography was first proposed by A. Fercher in 1995 as a variation of Fourier-Domain OCT [2] (Fig. 12.1). Technologies advocated and demonstrated at the time were in lack of robustness so as to be developed into viable and prac-

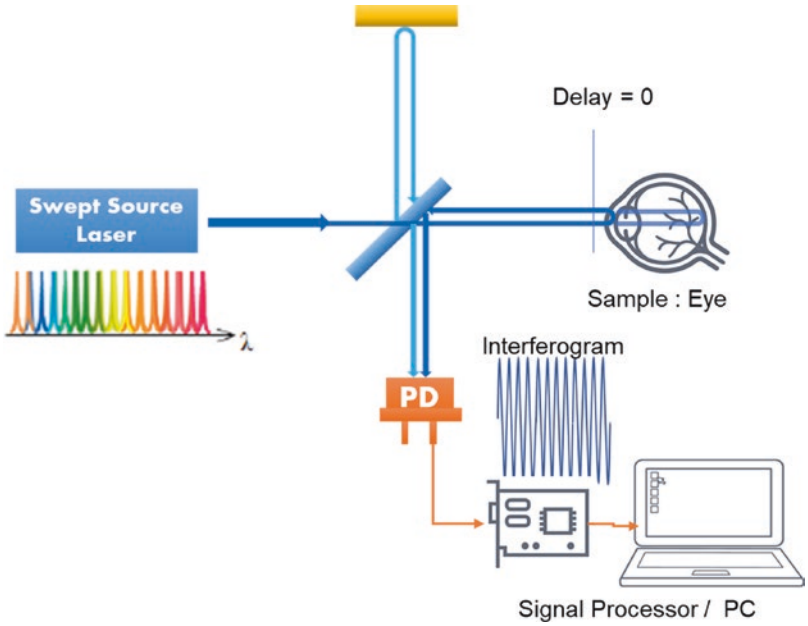

Fig. 12.1 Principle of swept-source OCT

C. Chong (✉)
Santec Holdings Corporation, Komaki, Japan
e-mail: changho.chong@santec.com

J. Aramberri et al. (eds.), *Intraocular Lens Calculations*, Essentials in Ophthalmology,
https://doi.org/10.1007/978-3-031-50666-6_12

tical applications. J. Fujimoto started to re-examine this approach in 2001 and thereafter many researchers followed and demonstrated faster imaging and higher sensitivity system over the course of years [3–7]. First commercial SS-OCT system was a 3D Anterior segment imaging system in 2008, Casia (Tomey, Nagoya, Japan) with a 30 kHz A-line rate which used high-speed-scanning laser (HSL-200, Santec Corporation).

Challenges

SS-OCT system boasts incomparable fast imaging speed due to fast swept rate of the laser wavelength change and high sensitivity due to intrinsically high signal efficiency based on Fourier transform in signal processing. Fast swept rate is an essential feature when imaging the large area with short acquisition time as well as overcoming the motion blur during the image acquisition. However, in order to realize the continuous wavelength sweep at the rate of 10 kHz to several hundred kHz, the other performance comes at a cost. Narrow spectral width which is conversely defined as "coherence length" of laser cannot be sustained as "long" enough as the laser that oscillates at stationary wavelength. As a result, imaging depth is limited to the order of a few millimeters because of its short coherence length. Researchers attempted many different approaches [3–7] to overcome this trade-off to achieve (1) continuous sweep with (2) large coherence length (narrow spectral width) during (3) faster swept rate, all simultaneously. For most of the applications, point of interest resides in subsurface of biological tissues such as in retinal imaging, or cancer assessment, two to five millimeters of coherence length was sufficient to serve as diagnostic modality as seen in Fig. 12.2.

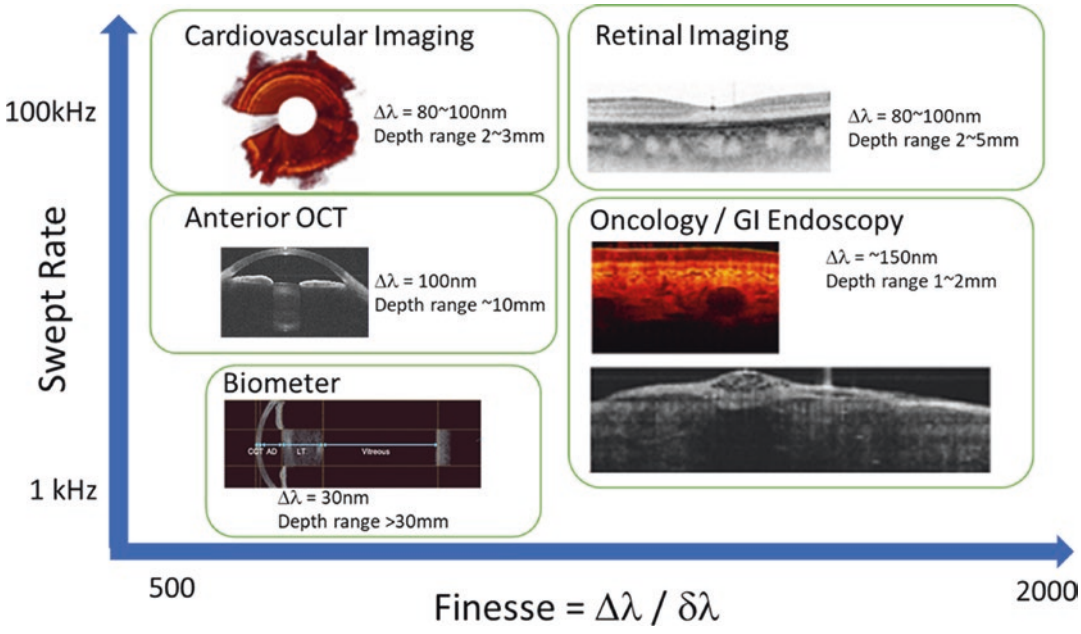

Fig. 12.2 Swept rate requirement in different clinical applications

Large Coherence Length

Coherence length of an SS-OCT system is defined by the optical path length difference between interferometer's sample path and reference path (see Fig. 12.1) where signal decays 6-dB (one-fourth) compared to nominal signal at zero path length or optical delay. And in the conventional definition, a half of coherence length corresponds to physical imaging depth in the system where signal amplitude, in the other words, image contrast is worsened by 6-dB. This doesn't necessarily mean image is cropped at this depth. Image is still visible as long as contrast is sufficient to reveal the lesion of interest.

$$\text{Coherence length} = \frac{2\ln 2\lambda_0^2}{\pi\delta\lambda}$$

Swept-Source Biometer

Early Work and Breakthrough

As advocated by Lexer et al. [8], the first demonstration of swept-source-based interferometer was indeed for the biometer application (see Fig. 12.3) in one-dimensional measurement. This was realized by the setup using a single longitudinal mode laser which has intrinsically narrow spectral width despite its slow wavelength tunability.

In order to overcome the increased output linewidth at higher scan rates, several ideas have been introduced such as the phase matching technique using an acousto-optic filter that matches the wavelength shift over a round trip to the phase shift generated by the filter itself [6]. Another technique is Fourier domain mode locking (FDML), whereby the tunable filter scan frequency is matched to the optical round-trip time resulting in a higher Q factor of the cavity in frequency domain [7, 9]. These two approaches, however, require both to operate at a preset resonant condition, i.e., at fixed swept rate, and the latter case needs long fiber length to accommodate several tens of kHz swept rate or slower. Other than using these techniques, adding the ambiguity or complex conjugate removal by adding external phase shifter in the OCT system is known as an alternative way [10], but it is not preferable when the system design is cost-sensitive.

After a decade later since the Lexer's demonstration in one-dimensional biometer at very slow speed, author's group demonstrated 28 mm coherence length at 2.5 kHz swept rate [12] using the method called Quasi-Phase Continuous Tuning technique [11] (Fig. 12.4) and achieved successful two-dimensional OCT of whole eye.

To our knowledge, this was the first demonstration of imaging whole eye of porcine with SS-OCT (Fig. 12.5).

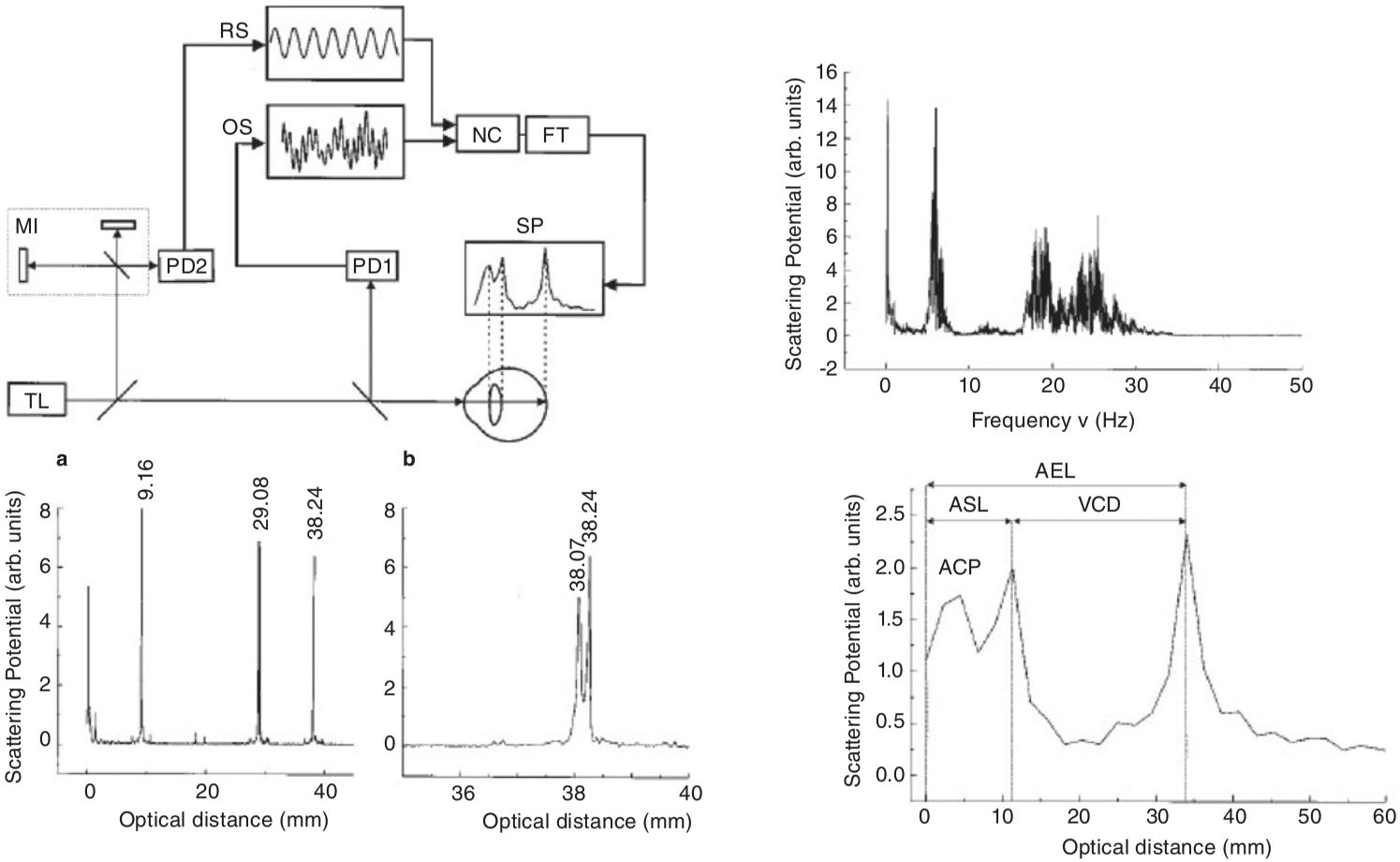

Fig. 12.3 First demonstration of axial length measurement (Lexer et al. [8]). Top left: Scheme of the WTI: wavelength tuning interferometer. *TL* tunable laser, *NC* numerical correction, *FT* Fourier transform. Top right: WTI scan of an eye model with 9 nm tuning. Bottom left: WTI scan of an eye model after numerical correction. Bottom right: WTI scan of a human eye in vivo obtained by high-speed piezotuning over 0.15 nm

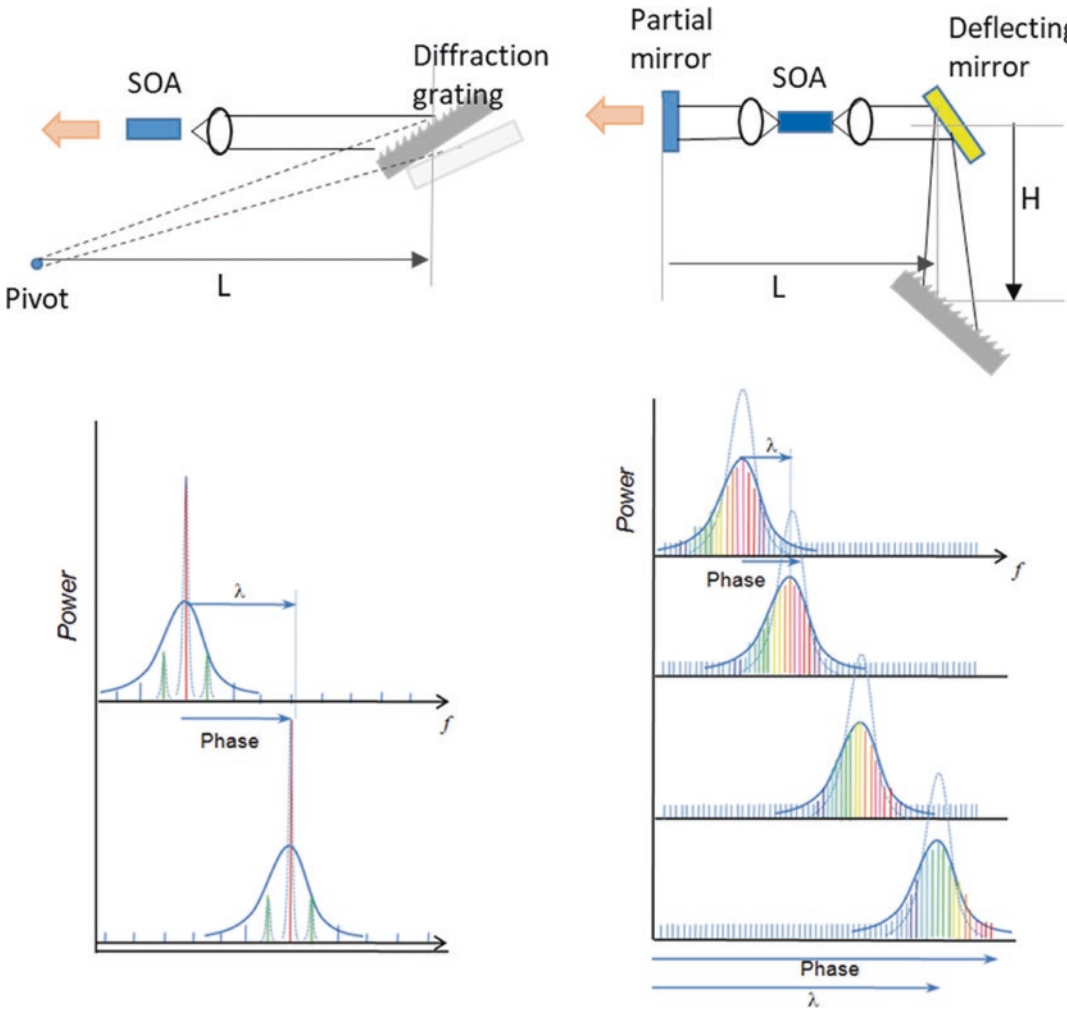

Fig. 12.4 Conceptual diagram for Quasi-Phase Continuous Tuning [11]

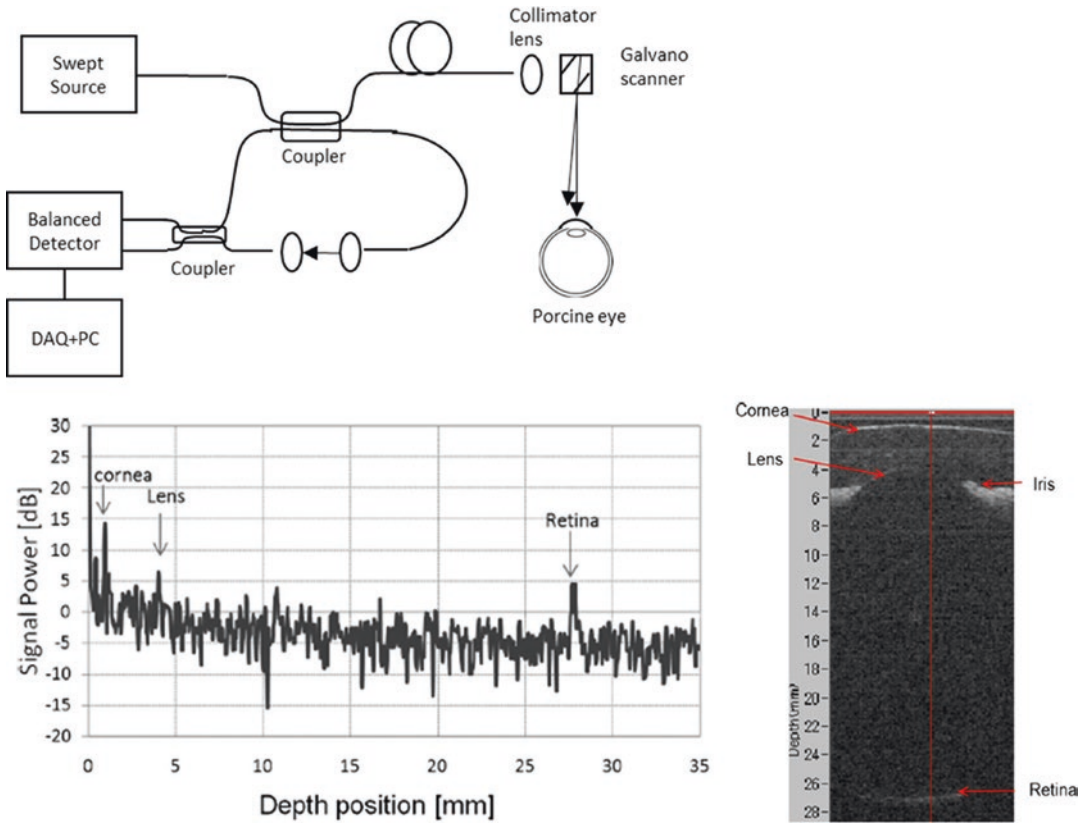

Fig. 12.5 First demonstration of whole eye imaging [12]

Argos SS-OCT Biometer

Basic Performance

Argos was first introduced to the market in 2014 in annual conference of ESCRS (European Society of Cataract & Refractive Surgeons) in London. ARGOS uses a proprietary swept-laser source (Santec Corp., Komaki, Japan) designed for deep (>50 mm) imaging at a fast 3000 lines/s A-line rate. Argos's performance specifications are listed in Fig. 12.6.

ARGOS is a swept-source OCT that captures an image of the whole eye from the cornea to the retina prior to cataract surgery. The measured image is used to calculate the biometric parameters necessary for IOL power calculation.

High Success Rate

The swept-source OCT technique for biometry delivers various advantages over traditional optical biometer as well as other non-contact techniques. First, the 1050 nm light used experiences less scatter than shorter wavelengths leading to more photons being available to make the measurement as seen in Fig. 12.7. Second, this technique has an inherent sensitivity advantage over other interferometric techniques. In addition, for ARGOS, the measurement beam scans across the eye capturing a full 2D image of the anterior chamber. For dense localized cataracts, this scanning helps ensures light travels past the cataract to reach the retina so that axial length can be measured. ARGOS even measures the densest

Parameter	Symbol	Range	Repeatability(s)
Central Corneal thickness	CCT	300-800 μm	< 10 μm
Anterior Chamber Depth	ACD	1.5-5.0 mm	10 μm
Lens Thickness	LT	0.5 – 6.5 mm	20 μm
Axial Length	AL	15 – 30 mm	10 μm
Corneal curvature	R_1, R_2(K_1, K_2)	5.5 – 10 mm (60-34D)	20 μm (0.13D)
Corneal Diameter	CD	7 – 15 mm	60 μm
Pupil Size	PS	2 – 13 mm	90 μm
Astigmatism angle	AST	0 – 180 deg	5deg (Cyl >1D)

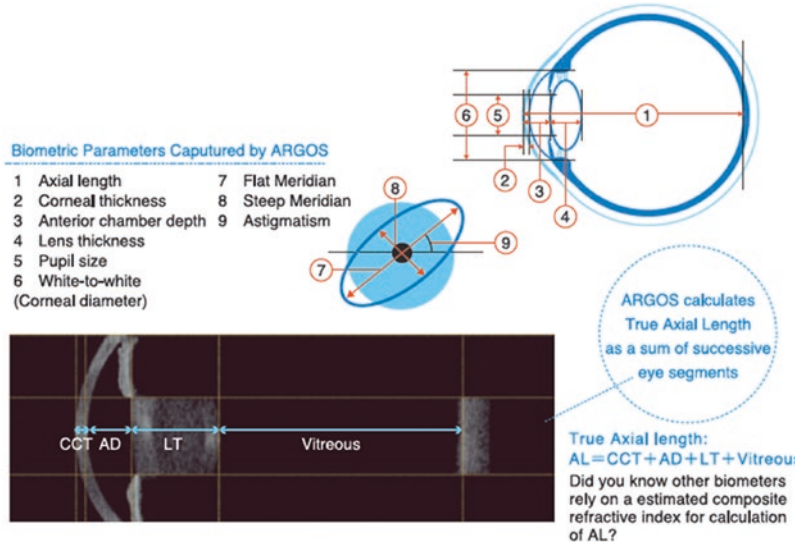

Fig. 12.6 SS-OCT biometer ARGOS

cataracts that usually require the use of ultrasound A-scan. Furthermore, faster real-time OCT imaging during alignment ensures the confidence of fixation and provides assurance of accurate measurement with instant validation.

ERV Mode

The Fourier domain techniques as applied to optical coherence tomography (OCT), such as spectral domain OCT (SD-OCT) and swept-source OCT (SS-OCT), rely on the basis of an immovable mirror that creates a window where interference is possible, thereby also defining the OCT image. The information contained in this window is encoded in spatial or temporal frequencies, depending on if the technique is spectral domain (SD-OCT) or swept-source (SS-OCT). It is only after performing the Fourier transform that it is possible to transform the frequencies (spatial or temporal) into spatial information. The window position depends on the position of the mirror, while the axial range of information depends on the bandwidth of the light source (coherence function). The amount of information, encoded in frequencies, depends on the ability to collect them: in SD-OCT, the separation power of the diffraction grating and the pixel size of the camera; in SS-OCT, the sampling of the signal. In the "normal mode," the coherence function is centered before the cornea, while in the "Enhanced Retinal Visualization" (ERV) it is centered closer to the retinal region. The intensity of the obtained image depends on the intensity of the backscattered light from the

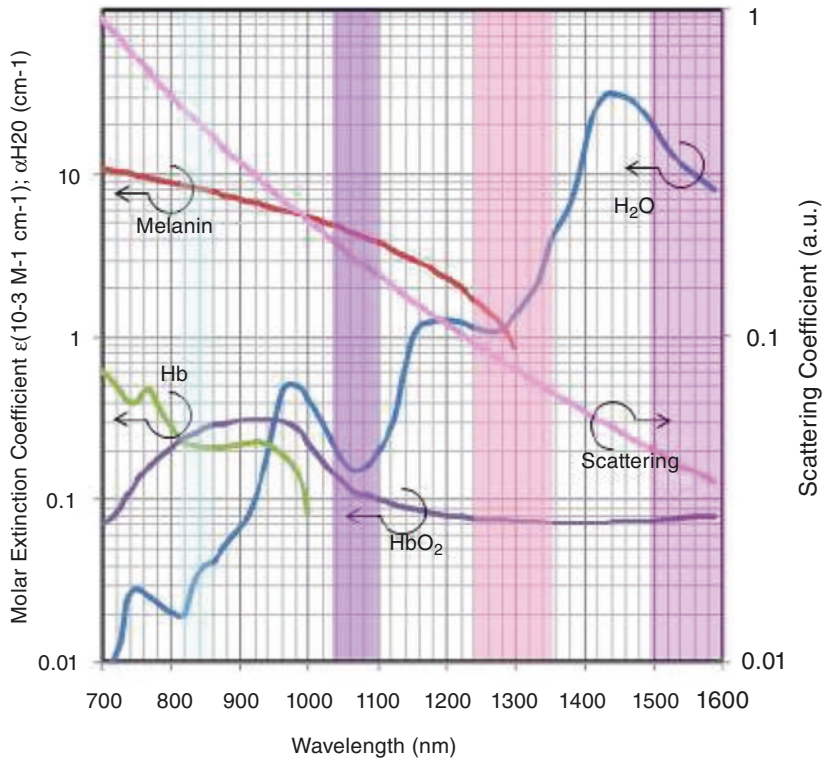

Fig. 12.7 Absorption and scattering coefficient of water

eye structures and their positions such that the acquired signal is the result of the convolution of the backscattered signal and the coherence function. When a dense cataract is present, the backscattered signal from the lens can partially or completely block the light coming back from the retina. In the normal mode, when the signal is convolved with the coherence function to produce the acquired signal, the retina can be hardly or not visible at all. However, in the ERV mode, the use of a shifted coherence function (due to the movement of the mirror) provides an additional opportunity to visualize the retina and therefore on evaluating the axial length (AL). In Fig. 12.8a–d, a conceptual image of the acquired signal of the system is shown. The backscattered signal from a cataract patient (one A-scan, i.e., columns of the image) is depicted in red. The coherence function is represented in blue and the acquired signal in black. (a) Simulated backscattered signal and normal coherence function (blue solid line). (b) Normal mode acquired signal (black solid line). (c) Simulated backscattered signal and ERV coherence function (blue dashed line). (d) ERV acquired signal (black dashed line). While this feature has been denominated as "Enhanced Retinal Visualization," it is not restricted to only dense cataracts or is it suggested to be used on all dense cataracts that may be encountered by the operator. Figure 12.8e–h present two cases from two different patients where the use of the ERV mode can be recommended. Top case: Retina not visible. (e) Normal mode where retina is not visible. (f) ERV mode where the retina is visible and AL can be evaluated. Bottom case: Retina appears fragmented. (g) Normal mode where retina appears fragmented and retinal signal is faint. (h) ERV mode where the retina is clearly visible and retinal signal is stronger. ERV boosts about 8–10 dB sensitivity to detect the retinal segment that compensates the signal decay by coherence length in normal mode so that it could make successful measurement in the densest cataract.

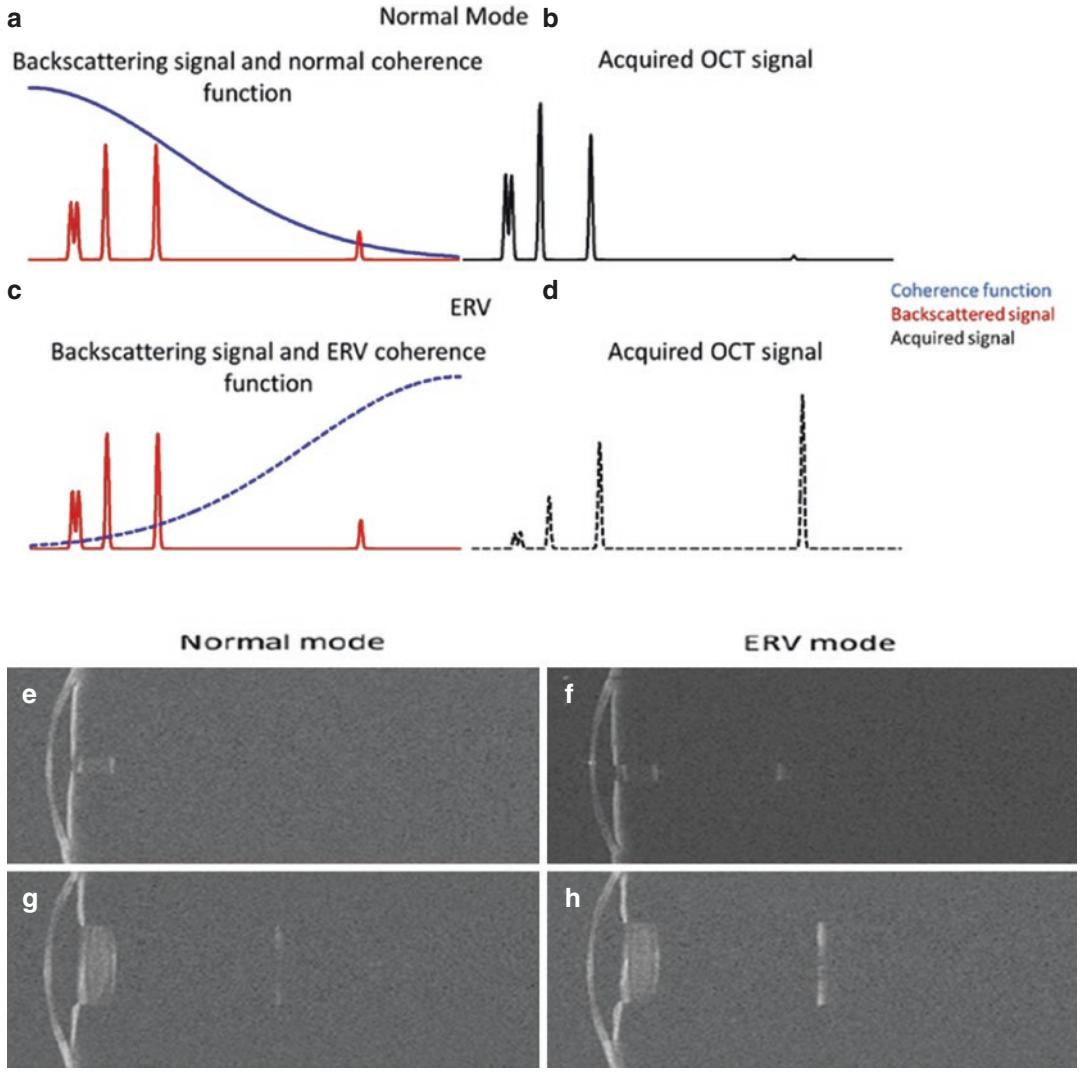

Fig. 12.8 ERV mode measurement

True Axial Length

In many of early clinical studies showing comparison of Argos, the conventional optical biometers tend to overestimate axial length at larger end, underestimate at shorter end, which is primarily the reason for not being able to predict short/long eyes with good precision in the past. Additional adjustment to the AL value calculated by tradition biometers is required to take into account the offset from true AL value before substituting to IOL power formula.

Argos calculates axial length as the sum of physical distances of four segments: central corneal thickness, aqueous depth, lens thickness, thickness of vitreous humor to the retina each calculated by dividing optical distance by corresponding refractive indices (1.375, 1.336, 1.41, 1.336) at infra-red wavelength range which implies the true physical scale of AL (Fig. 12.9). On the other hand, the conventional biometer uses composite refractive index where a statistically average proportion of axial length to lens thickness is assumed [13]. This approach does

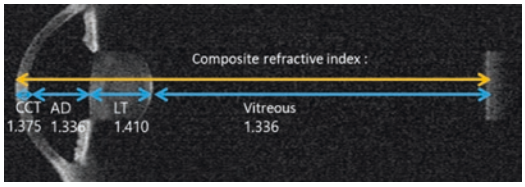

Fig. 12.9 True axial length—sum of segmented optical length

not take into account the actual lens thickness that could be out-of-proportion from normal distribution.

Composite refractive index used in traditional optical biometers was calibrated against ultrasound A-scan biometer's measurement. However, it is important to note that ultrasound and light have completely different behavior. Ultrasound travels faster in dense material while light travels slower in denser medium. The average composition or ratio of lens thickness to axial length is believed to be around 20%, and it decreases as the axial length is larger than average AL of 23.5 mm, which means total density gets lowered; thus, ultrasound travels slower and light travel faster. If a biometer is calibrated against ultrasound-based biometer and taken with average axial length demography, composite refractive index and formula for adjustment will reflect this effect in a linear extrapolated manner. That means it assumes the ratio of lens to AL is linear proportional to AL. So, what if lens thickness is disproportionate when axial length is large? The most Asian adults have a larger axial length compared to people in western country. And quite a few people have larger than "average" lens thickness which doesn't follow the linearly extrapolated distribution. If one applies formula based on composite refractive index, or IOLMaster (Zeiss Meditec, Germany) based value, it overestimates AL in the case of larger lens thickness because the device assumes it is measuring the eye with lens with smaller ratio while it is not. Wang and Koch did the studies on population with the eye with longer AL to account for this discrepancy and proposed adjustment which is also linear extrapolation. However, the distinction between overestimated AL and apparently true AL is difficult for users to judge according to intended use of the device. It is confusing for users whether AL output is actually true or overestimate and whether device is correcting for either of cases. Without knowing it, additional adjustment is simply a bet based on statistics.

$$\mathrm{AL}_{\mathrm{ARGOS}} = \frac{\mathrm{CCT}}{1.375} + \frac{\mathrm{AD}}{1.336} + \frac{\mathrm{LT}}{1.41} + \frac{\mathrm{Vitreous}}{1.336} - \text{Retinal thickness offset} \tag{12.1}$$

$$\mathrm{AL}_{\mathrm{IOLMaster}} = \frac{\left(\frac{\mathrm{OPL}*}{1.3549} - 1.3033\right)}{0.9571} \tag{12.2}$$

Figure 12.10 shows the distribution of the ratio of lens thickness to true axial length measured by ARGOS. Linear approximation in red represents interpretation of proportion that traditional optical biometer is considering.

Assuming this linear approximation of LT/AL found, $y = -0.0149x + 0.5513$, whereas y is LT/AL and x is AL, is ground-truth data of proportion, let's mathematically estimate both the composite refractive index of whole eye and composite ultrasound velocity by weighing the refractive indices of crystalline lens (1.410) and vitreous (1.336), respectively, as well as sound velocity, 1641 m/s for lens and 1532 m/s for vitreous in the same way.

$$\text{Composite Refractive Index} : n(y) = 1.41y + 1.336(1 - y) \tag{12.3}$$

$$\text{Composite Sound Velocity} : v(y) = 1641y + 1532(1 - y) \tag{12.4}$$

If the weight, $y = -0.0149x + 0.5513$, is substituted, they become as following forms:

$$\text{Composite Refractive Index} : n(x) = -0.0011x + 1.3767 \tag{12.5}$$

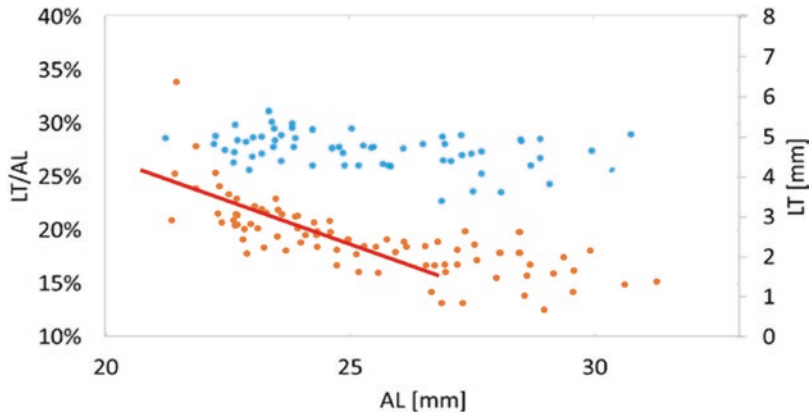

Fig. 12.10 The ratio of lens thickness to axial length of the eye (conceptual image of actual data)

$$\text{Composite Ultrasound Velocity}: v(x) = -1.6241x + 1592 \tag{12.6}$$

"True" AL should be adjusted by multiplying a factor of $n(x)/n(23.5)$ which is the difference of refractive index at AL = x with respect to the refractive index at nominal of 23.5 mm. In the same way, ultrasound velocity can be adjusted by multiplying $v(23.5)/v(x)$ in relative to those in average axial length, 23.5 mm. Total adjustment is the sum of these two factors:

$$\text{AL}_{\text{optical biometer}} = \text{AL}_{\text{measured}} + \left(\frac{v_0}{v(x)} + \frac{n(x)}{n_0} \right) \text{AL}_{\text{measured}} \tag{12.7}$$

whereas $v_0 = v(x = 23.5)$, $n_0 = n(x = 23.5)$, $\text{AL}_{\text{measured}}$ is the value of optical length measured divided by nominal refractive index (e.g., 1.3549 in Eq. 12.2).

When Eqs. (12.3) and (12.4) are substituted into Eq. (12.4) and approximated in the first order around x = 23.5 mm, equation is deduced to the following form:

$$\text{AL}_{\text{optical biometer}} = 1.043\text{AL}_{\text{measured}} - 1.005 \tag{12.8}$$

$$\text{AL}_{\text{IOLMaster}} = \frac{\left(\frac{\text{OPL}*}{1.3549} - 1.3033 \right)}{0.9571} = 1.045\left(\frac{\text{OPL}*}{1.3549} - 1.303 \right) = 1.045\left(\frac{\text{OPL}*}{1.3549} \right) - 1.36 \tag{12.9}$$

Coefficient of first term 1.043 is close to reciprocal of 0.9571 (1.045) in Eq. (12.2) suggesting the agreement of this assumption. This proves our assumption that the conventional optical biometers suffer the inherent issue with contradictory nature of speed of light and ultrasound velocity. The difference in the second term of Eqs. (12.8) and (12.9) is simply the offset of retinal thickness to account for IOL formula based on ultrasound.

Those eyes in the larger axial length over 25 mm as seen in the graph of Fig. 12.9, distribution spreads wider and becomes no longer correlated well with linear approximation; thus, it increases the ambiguity when the linear approximation is still used. This is not something resolved by machine learning techniques on top to cover it up if the measurement itself contains ambiguity. That is why it is important to measure true axial length.

A number of clinical studies were reported to prove clinical and statistical significance on the use of true axial length applied to IOL power determination [14].

Future of SS-OCT with Tunable VCSEL

VCSEL (Vertical Cavity Surface Emitting Laser) becomes now popular even in consumer electronics such as smartphones that use VCSEL for 3D

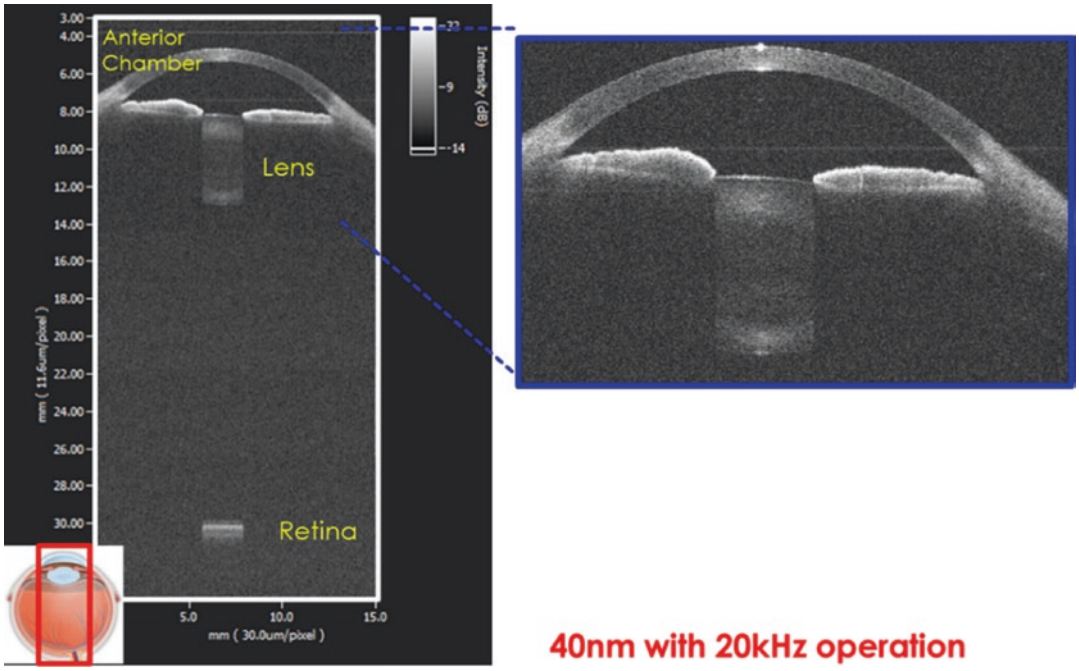

Fig. 12.11 SS-OCT whole eye image measured with tunable VCSEL

sensing for face recognition or lidar applications. Wavelength tunable version of this is the most coveted ultimate solution for the next generation SS-OCT [15, 16]. It boasts wide wavelength swept range of over 80 nm at 1050 nm band and intrinsically single-mode laser oscillation, thus very long coherence length. That means the depth range trade-off is no longer trade-off at faster swept rate. In fact, with integrated MEMS (Micro-Electro-Mechanical System) mirror enables several hundred kHz swept rate while maintaining large coherence length. One another advantage of tunable VCSEL that differentiate from the other swept-source is the reconfigurability of performance specifications. In the other words, one can software-define the swept range, swept rate in various required settings. Tunable VCSEL has a potential to bring multiple OCT functions in one device, for example, anterior OCT, optical biometer, and retinal OCT. Figure 12.11 shows the example image of in vivo human eye measured with a prototype that used a tunable VCSEL having the performance shown in Fig. 12.12.

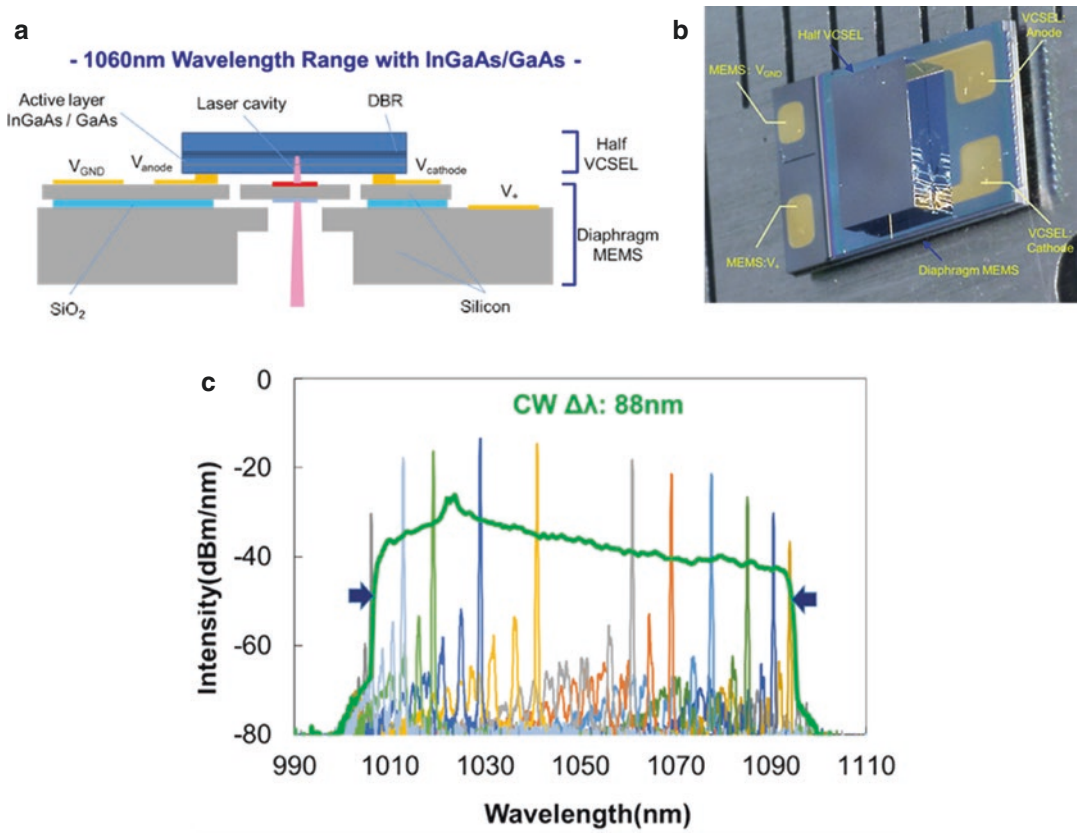

Fig. 12.12 Tunable VCSEL swept-source [15]. (**a**) Cross-sectional image of device structure, (**b**) an image of device, and (**c**) wavelength swept performance

References

1. Huang D, Swanson EA, Lin CP, Schuman JS, Stinson WG, Chang W, Hee MR, Flotte T, Gregory K, Puliafito CA, Fujimoto JG. Optical coherence tomography. Science. 1991;254:1178–81.
2. Fercher AF, Hitzenberger CK, Kamp G, Elzaiat SY. Measurement of intraocular distances by backscattering spectral interferometry. Opt Commun. 1995;117:43–8.
3. Chinn SR, Swanson EA, Fujimoto JG. Optical coherence tomography using a frequency-tunable optical source. Opt Lett. 1997;22:340–2.
4. Yun SH, Tearney GJ, de Boer JF, Iftimia N, Bouma BE. High-speed optical frequency-domain imaging. Opt Express. 2003;11:2953–63.
5. Yun SH, Tearney GJ, de Boer JF, Bouma BE. Motion artifacts in optical coherence tomography with frequency domain ranging. Opt Express. 2004;12:2977–98.
6. Yun SH, Richardson DJ, Culverhouse DO, Kim BY. Wavelength-swept fiber laser with frequency shifted feedback and resonantly swept intra-cavity acoustooptic tunable filter. IEEE J Sel Top Quant Electron. 1997;3(4):1087.
7. Huber R, Adler DC, Srinivasan VJ, Fujimoto JG. Fourier domain mode locking at 1050 nm for ultra-high-speed optical coherence tomography of the human retina at 236,000 axial scans per second. Opt Lett. 2007;32:2049–51.
8. Lexer F, Hitzenberger CK, Fercher AF, Kulhavy M. Wavelength-tuning interferometry of intraocular distances. Appl Opt. 1997;36(25):6548.
9. Srinivasan V, Huber R, Gorczynska I, Fujimoto J, Jiang J, Reisen P, Cable A. High-speed, high resolution optical coherence tomography retinal imaging with a frequency-swept laser at 850 nm. Opt Lett. 2007;32:361–3.
10. Yun SH, Tearney GJ, de Boer JF, Bouma BE. Removing the depth-degeneracy in optical frequency domain imaging with frequency shifting. Opt Express. 2004;12(20):4822–8.
11. Chong C, Suzuki T, Morosawa A, Sakai T. Spectral narrowing effect by quasi-phase continuous tuning

in high-speed wavelength-swept light source. Opt Express. 2008;16:21105–2118.
12. Chong C, Takuya S, Totsuka K, Morosawa A, Sakai T. Large coherence length swept source for axial length measurement of eye. Appl Opt. 2009;48(10):D144.
13. Haigis W, Lege B, Miller N, Schneider B. Comparison of immersion ultrasound biometry and partial coherence interferometry for intraocular lens calculation according to Haigis. Graefes Arch Clin Exp Ophthalmol. 2000;238(9):765–73.
14. John Shammas H, Ortiz S, Shammas MC, Kim SH, Chong C. Biometry measurements using a new large-coherence–length swept-source optical coherence tomographer. J Cataract Refract Surg. 2016;42(1):P50.
15. Okano M, Chong C. Swept source lidar: simultaneous FMCW ranging and nonmechanical beam steering with a wideband swept source. Opt Express. 2020;28(16):23898–915.
16. Khan MS, Keum C-D, Isamoto K, Sakai T, Doi T, Kawasugi M, Totsuka K, Chong C, Nishiyama N, Toshiyoshi H. High reliability electrically pump MEMS based widely tunable VCSEL for SS-OCT. In: SPIE photonics west, MOEMS and miniaturized systems XVIII; 2019. p. 10931–44.